PHYSICAL REVIEW B VOLUME 4, NUMBER 6 15 SEPTEMBER 1971

Studies of Vibrational Surface Modes. III. Effect of an Adsorbed Layer*

G. P. Alldredge, R. E. Allen, † and F. W. de Wette
Department of Physics, University of Texas, Austin, Texas 78712
(Received 3 March 1971)

The vibrational modes of adsorbate-substrate systems have been studied for models in which the adsorbate is simulated by a light or heavy monolayer. The monolayer is assumed to have the same structure and potential parameters as the substrate, and to differ only in particle mass. These models are more nearly realistic than those used in most previous treatments of this problem in that the structure of the substrate is fcc rather than simple cubic and, more important, in that the condition of rotational invariance is not violated. The (100), (111), and (110) surfaces have been treated. For each of these surface orientations, the vibrational modes have been calculated for mass ratios $M_L/M = 1/4$, 1/2, 4/5, 5/4, 2/1, and 4/1, where M_L and M are, respectively, the masses of adsorbate and substrate particles. The surface-dispersion curves are shown for each of these 18 cases, and the shifts in the surface-mode spectra with changes in the mass ratio are discussed. For very light or very heavy adsorbed particles, there are three principal surface-mode branches associated with the adsorbed layer which exist over all (for light particles) or nearly all (for heavy particles) of the two-dimensional Brillouin zone. For mass ratios which are not extreme, the separation of the principal surface-mode branches is not complete; at small wave vectors, some or all of these branches in effect enter the bulk bands as mixed modes (pseudosurface modes). As one expects, the first-layer modes are greatly affected by changes in the mass ratios. Second- and third-layer modes ordinarily are not much affected by increases in the mass ratio (heavy layer), but ordinarily are greatly affected by decreases in the mass ratio (light layer). The effect of the adsorbed layer on the localization of the generalized Rayleigh waves is examined; for these waves, heavy adsorbed layers enhance localization at the surface and light layers have the opposite effect.

I. INTRODUCTION

In this paper the work of the preceding papers I[1] and II[2] is extended to a study of the effects of an adsorbed layer on the surface-mode frequencies of a slab-shaped crystal. The effects of defect atomic layers on crystal surfaces have been studied theoretically for one- and two-dimensional geometries[3–5] and for simple-cubic crystals[6–9] in three dimensions. More recently, Dobrzynski has calculated the localized-mode frequencies of adsorbed atoms ("adatoms") on the (100) surface of a body-centered cubic crystal.[10]

Much of the previous theoretical work on surfaces of three-dimensional crystals has been based on variations of the "Rosenstock-Newell-Montroll-Potts" model. An unfortunate side effect of the simplifications provided by this model is the violation of a fundamental rigid-body rotational invariance requirement,[11] and in monatomic crystals this leads to a complete absence[5] of the long-wavelength surface waves—the generalized Rayleigh waves—which are essential characteristics in the vibrational properties of pure surfaces. The work of Refs. 5 and 10 and of the present authors utilizes models that do satisfy the required rotational invariance. Consequently, modifications of the Rayleigh surface and pseudosurface wave branches due to the presence of an adsorbed layer can be, and are here, explored.

In Sec. II we present the results of an extensive set of calculations of surface-vibrational properties of a model simulating an adsorbed monolayer on several faces of a monatomic fcc crystal. The model may be termed a "simple mass-defect model" in that the adatoms differ from bulk atoms only in mass. Thus the adsorbed layer has the same structure and lattice spacing as the substrate; however, distortions near the surface due to the presence of the surface and the consequent changes in atomic-force constants are taken into account as they have been for the pure surface.[2] In Sec. II, we outline the method of calculation, summarizing those elements of Paper I[1] required for an understanding of the present paper, and in Sec. III results for the (100), (111), and (110) surfaces are presented. (A calculation of the thermodynamic functions and the Debye-Waller factor for the present model has been reported elsewhere,[12] and some results of the present study have appeared previously.[13]) Section IV summarizes the most important findings of the present paper.

II. FORMULATION

The general method of calculation has been described in detail elsewhere,[1,2,14] so only an outline will be given here to establish notation and to describe the particular features of the model used.

This simple mass-defect model is identical to that used in our studies of monatomic crystals, except that the atoms in the surface layer are considered to be adatoms whose mass differs from that of the bulk atoms. The mass of an adatom is denoted M_L, and the mass of a substrate atom, M. All atoms are assumed to interact through a Lennard-Jones potential of the form

$$\phi(r) = 4\epsilon\left[(\sigma/r)^{12} - (\sigma/r)^{6}\right], \tag{2.1}$$

where ϵ, σ, and r are, respectively, the energy parameter of the potential, the core-radius parameter, and the interparticle distance. The parameters M, ϵ, and σ define a "natural" system of units for the model; the frequencies reported in this paper will be referred to this scale of units $[\omega^* \equiv \omega \times (\epsilon/M\sigma^2)^{-1/2}]$. The density of the bulk crystal is fixed by the value of the ratio $\sigma/a = 1.297$, where $2a$ is the usual cubic-lattice constant. At this density, the static energy of the crystal in bulk is minimized, and the bulk elastic constants are

$$c^*_{11} = 96.8, \qquad c^*_{12} = c^*_{44} = 55.3, \tag{2.2}$$

where

$$c^*_{ij} \equiv c_{ij}/(\epsilon\sigma^{-3}).$$

The problem of the surface-boundary conditions is dealt with by considering the system to be a slab of N_3 atomic planes of the same structure and stacked appropriately for the surface being considered. The interplanar spacings near the two free surfaces are allowed to relax from their bulk value[14]: the resulting static-equilibrium configuration leads to modification of the interatomic force constants near the surface, resulting in characteristic features in the surface modes.[2] The equilibrium position of an atom is written as[15]

$$\vec{r}_0(\vec{l}) = \bar{r}_0^{\bar{l}} + \vec{r}_0(l_3), \tag{2.3}$$

where the position $\bar{r}_0^{\bar{l}}$ of the point $\bar{l} = (l_1, l_2)$ of the two-dimensional lattice (diperiodic net) is given in terms of the primitive-lattice vectors $\bar{a}_1$ and $\bar{a}_2$ of the surface net of the particular surface,

$$\bar{r}_0^{\bar{l}} = l_1\bar{a}_1 + l_2\bar{a}_2, \tag{2.4}$$

and where each of the N_3 planes is labeled by the index l_3. The "basis vector" $\vec{r}_0(l_3)$ has components not only in the direction normal to the surface, but may have a nonzero projection $\bar{r}_0(l_3)$ on the surface as well [e.g., the fcc stacking of (111) planes is in an order $ABCABC\ldots$, and if the origin of the net is placed on an A-plane atom $[\bar{r}_0(l_3 = 0, 3, \ldots) = 0]$, then $\bar{r}_0(l_3 = 1, 4, \ldots) = \bar{r}_{0B} \neq 0$ and $\bar{r}_0(l_3 = 2, 5, \ldots) = \bar{r}_{0C} \neq 0$].

The harmonic equations of motion for the crystalline slab are

$$M(l_3)\frac{d^2}{dt^2}u_\alpha(\vec{l}) = -\sum_{\vec{l}',\beta}\Phi_\alpha(\vec{l},\vec{l}')u_\beta(\vec{l}')$$

$$(\alpha = x, y, z), \tag{2.5}$$

where $\vec{u}(\vec{l}) = \vec{r}(\vec{l}) - \vec{r}_0(\vec{l})$ is the time-dependent displacement from equilibrium, and the force constants $\Phi_{\alpha\beta}(\vec{l},\vec{l}')$ are derived from Eq. (2.1) in the usual way.[14] Corresponding to the diperiodicity of the surface net, there is a two-dimensional reciprocal space in which the wave vectors of propagation $\bar{q}$ are defined. The normal-mode solutions of Eq. (2.5) have the form

$$u_\alpha(\vec{l}) \propto [M(l_3)]^{-1/2}\,\xi_\alpha(l_3)\exp[i\bar{q}\cdot\bar{r}_0(\vec{l}) - \omega t], \tag{2.6}$$

which reduces Eq. (2.5) to the dynamical matrix eigenvalue equation

$$\sum_{l_3',\beta} D_{\alpha\beta}(l_3, l_3'; \bar{q})\xi_\beta(l_3'; \bar{q}p) = \omega_p^2(\bar{q})\xi_\alpha(l_3; \bar{q}p), \tag{2.7}$$

with

$$D_{\alpha\beta}(l_3, l_3'; \bar{q}) = [M(l_3)M(l_3')]^{-1/2}\sum_{\bar{l}'}\Phi_{\alpha\beta}(l_3, l_3'; \bar{l}')$$

$$\times\exp\{i\bar{q}\cdot[\bar{r}_0^{\bar{l}'} + \bar{r}_0(l_3') - \bar{r}_0(l_3)]\}. \tag{2.8}$$

The index p is a generalized polarization label for the $3N_3$ normal modes obtained for each $\bar{q}$. The eigenvectors in the results presented in Sec. III are orthonormal:

$$\sum_{l_3,\alpha}\xi_\alpha(l_3; \bar{q}p)\xi_\alpha^*(l_3; \bar{q}p') = \delta_{pp'}. \tag{2.9}$$

III. RESULTS

In this section we present the calculated vibrational modes of fcc slabs bearing adsorbed monolayers, having (100), (111), and (110) orientations, and having a thickness of $N_3 = 21$ atomic planes, including the adsorbed monolayers. The discussion is keyed to the results of Ref. 2 for the pure surfaces, with emphasis on the effects of the adsorbed layer on the modes of the pure surface.

The frequencies and eigenvectors of the dynamical matrix of the slab bearing an adsorbed monolayer on each of its two outer surfaces are obtained by numerical solution of Eq. (2.7). The frequencies are displayed as surface-dispersion curves (e.g., Fig. 2) for the $\bar{q}$ vector tracing out circuits around the irreducible elements of the two-dimensional or diperiodic Brillouin zones (DBZ) shown in Fig. 1. (Typical irreducible elements of the DBZs are emphasized by heavy lines.) The curves are computer generated, with modes for neighboring $\bar{q}$ vectors connected in strictly increasing order. By inspection of the l_3 dependence of the eigenvec-

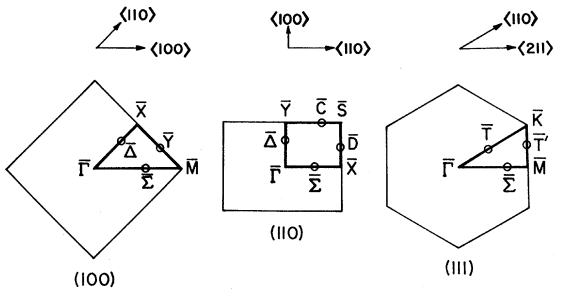

FIG. 1. Diperiodic Brillouin zones (DBZ) for the (100), (110), and (111) surfaces of the fcc crystal. Typical irreducible elements are outlined by heavy lines, and special symmetry points and lines are labeled according to a scheme adapted for two dimensions (Ref. 1) from Koster's compilation. A key to the principal in-plane directions appears above each DBZ. The scales are given by the following: For the (100) DBZ, $\bar{q}_{\bar{X}} = (\pi/a\sqrt{2})\,(0,1,1)/\sqrt{2}, \bar{q}_{\bar{M}} = (\pi/a)\,(0,0,1)$; for the (110) DBZ, $\bar{q}_{\bar{X}} = (\pi/a\sqrt{2})\,(-1,1,0)/\sqrt{2}$, $\bar{q}_{\bar{Y}} = (\pi/a)\,(0,0,1)$; for the (111) DBZ, $\bar{q}_{\bar{M}} = (\pi\sqrt{6}/3a)\,(1,1,-2)/\sqrt{6}$, $\bar{q}_{\bar{K}} = (2\pi\sqrt{2}/3a)\,(0,1,-1)/\sqrt{2}$.

tors $\bar{\xi}(l_3)$, the surface and pseudosurface modes are identified. The proper connectivity was established only for the surface-mode branches.

Surface- and pseudosurface-mode branches appear in the dispersion-curve plots as pairs of curves that are degenerate or nearly degenerate for $|\bar{q}| \gtrsim 0.1\,\bar{q}_{BZ}$, since for the slab the surface-localized modes are, to zeroth order, degenerate pairs of linear combinations of the waves localized on each of the two surfaces of the slab.[1] For $\bar{q}$ nearer the origin $\bar{\Gamma}$, the degeneracy of surface-mode pairs existing in this region is increasingly split due to the finite thickness of the slab.

Before discussing the effects of the adsorbed monolayer on the vibration of the various surfaces, we summarize the salient features of the vibrational modes for pure surfaces, i.e., (i) the bulk bands and gaps within them and (ii) the rich variety of surface-mode branches associated with edges of the bulk bands.[2] The bulk modes are distributed in quasicontinuous bands. The amplitude of each bulk mode of the slab varies with $\bar{l}$ as that of a wave propagating with wave vector $\bar{q}$, and may roughly be considered to vary with l_3 as that of a standing wave with a wave vector q_3. Thus at any fixed value of $\bar{q}$, the bulk modes fall into a quasicontinuum of frequencies as q_3 ranges over its domain of values. The bulk bands are delimited below[16] and above, but in addition there are gaps *within* the bulk bands.[17] We may label these gaps by prominent surface-mode branches that appear in them,[2] e.g., the "$S_6(100)$ gap" (see below). One may observe features in the bulk bands corresponding to waves in the infinite crystal having $q_3 = 0$ and hence propagating parallel to the surface of the slab.[18]

The surface-mode branches that appear in the case of pure surfaces are labeled S_i according to an arbitrary scheme for each surface.[2] The index of the particular surface may be appended when necessary to prevent confusion between surface branches having the same label but belonging to different surfaces, e.g., modes $S_7(100)$ and S_7 (110) have no apparent relation to each other, while modes $S_6(100)$ and $S_7(110)$ do seem to be related (see Sec. III C of Ref. 2).

The fact that there usually are surface branches associated with bulk band edges—including those that are boundaries of the intraband gaps—contributes to the rich variety of surface branches. Furthermore, in addition to the surface waves in which the maximum amplitude is in the outermost layer with diminishing amplitude deeper into the crystal, there are "second-layer" surface modes in which the peak amplitude is in the second layer with subsequent attenuation into the crystal. Indeed, it appears that the usual case is that the various surface-mode branches exist in families,[2] each family a series of first-, second-, ..., mth-layer modes in which the higher-order–layer modes exist closer and closer to the associated bulk band edge and hence exist over a smaller and smaller region of the DBZ. These higher-order surface modes usually are highly dependent on there being changes in the force constants near the surface.[2,19] [A notable exception is $S_7(100)$.[20]] The present discussion is primarily focused on a selection of first- and second-layer surface modes.

In considering surface-mode branches that appear only when an adsorbed layer is present, we label such branches A_i for the case of light adatoms and A_i' for heavy adatoms; the assignment of the index i for $i > 3$ is according to an arbitrary scheme, while the values $i = 1, 2, 3$ are reserved for members of the set of "principal adsorbed-layer surface branches," defined as follows. We find that at the extremes of adatom mass there are three surface-mode branches which are associated with the presence of the adsorbed monolayer, which exist well into the small-$\bar{q}$ region, and which have shapes reminiscent of that of the bulk bands. These three surface branches we call principal adsorbed-layer surface branches. They lie above the bulk bands in the light adatom extreme and are labeled A_1, A_2, and A_3; in the heavy adatom extreme they lie below the bulk bands and are labeled S_1, A_2', and A_3' for the (100) and (111) surfaces. The three principal adsorbed-layer surface branches for the (110) surface with heavy adatoms retain the labels S_1, S_2, and S_3 assigned for the pure surface, since all three of these small-$\bar{q}$ surface modes are observed for the pure (110) surface.

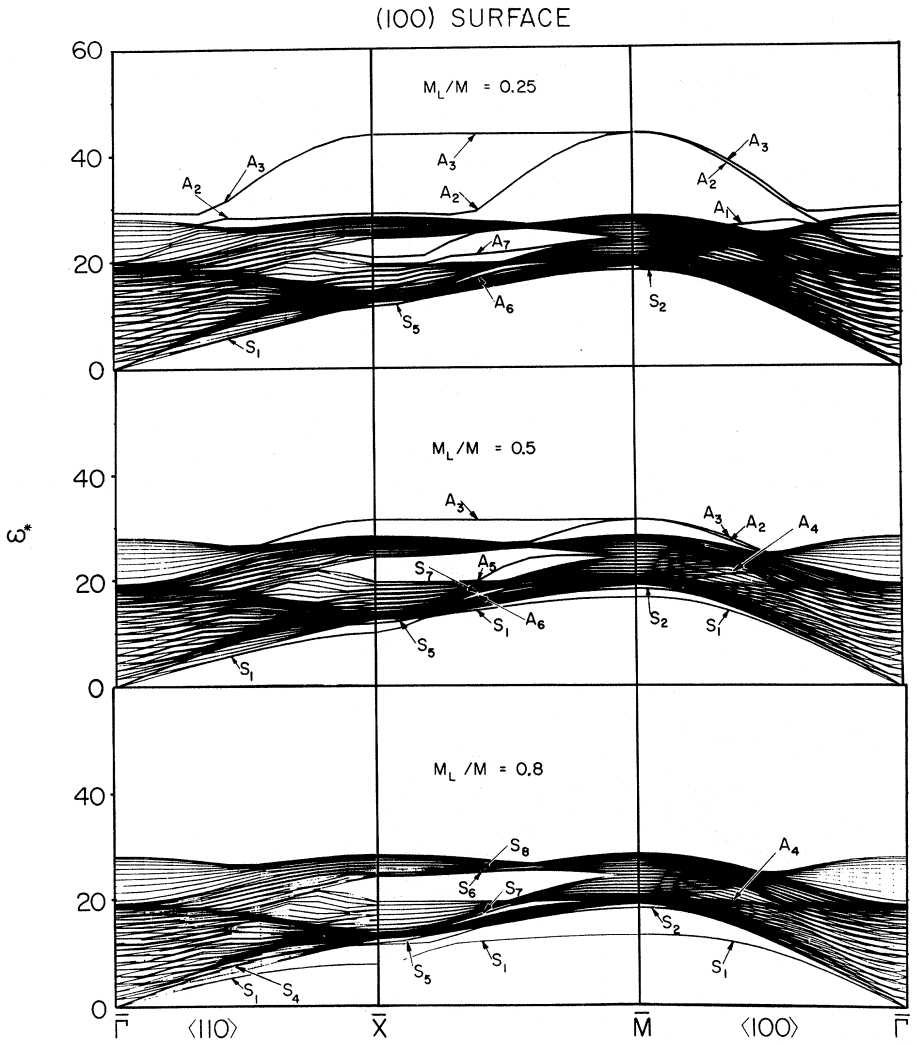

FIG. 2. Surface-dispersion curves of the fcc (100) slab, with adatom mass M_L less than that of substrate atoms, M. The abscissa scale of the segment $\bar{M}\bar{\Gamma}$ has been reduced by a factor of $2^{-1/2}$ relative to the $\bar{\Gamma}\bar{X}$ and $\bar{X}\bar{M}$ segments.

A. (100) Surface

Figures 2 and 3 exhibit the surface-dispersion curves for the fcc (100) surface for decreasing values of M_L/M (ratio of adatom mass to substrate atom mass) (Fig. 2) and for increasing M_L/M (Fig. 3). Before discussing the effects of the adsorbed layer, we summarize the salient features of the surface-dispersion curves for the pure (100) surface.[2] The sagittal plane—the plane containing the normal to the surface and the wave vector $\bar{q}$—is a plane of reflection symmetry for $\bar{q}$ along the lines $\bar{\Gamma}\bar{X}$ (⟨110⟩) and $\bar{\Gamma}\bar{M}$ (⟨100⟩). Consequently, all modes, bulk and surface, partition[1] into modes characterized by polarizations in the sagittal plane (two-thirds of all modes) and by polarization normal to the sagittal plane (one-third of all modes). The latter polarization we may term shear horizontal (SH) in analogy to usage in seismology[21]; the sagittal-plane polarizations—although generally elliptical—are frequently either predominantly parallel to $\bar{q}$ or predominantly normal to the surface such that they may be characterized qualitatively as a primarily longitudinal mode (P) or a shear vertical mode (SV), respectively. The gaps in the bulk bands for the fcc (100) surface are the trivial S_1 (100) gap lying below the bottom edge of the complete bulk bands, the S_6 (100) gap near $\bar{X}$ and along most of the boundary of the DBZ, the narrow S_7 (100) gap seen between $\bar{X}$ and $\bar{M}$ on the DBZ boundary, and the S_3 (100) quasigap that is seen to open and close along $\bar{\Gamma}\bar{M}$.

By quasigap we mean a gap in one bulk subband [e.g., for the S_3 (100) quasigap, the subband polarized in the sagittal plane] which is overlapped by other bulk subbands (in this example, the SH bulk subband) whose polarizations are at least approximately decoupled from the polarizations of the first subband. These quasigaps are ordinarily associated with symmetry elements—usually mirror planes

such as that along $\bar{\Gamma}\bar{M}$—along which the decoupling of polarizations is rigorous. When a wave vector $\bar{q}$ in such a gap along a symmetry element swings away from the symmetry element, the decoupling of polarizations becomes only approximate, with the approximation becoming worse the greater the deviation of $\bar{q}$ from the symmetry element. It is useful to consider these regions of approximate decoupling of polarization as quasigaps even when the symmetry element is not quite present (see the discussion of the $\bar{\Gamma}\bar{S}$ direction in Sec. III C of Ref. 2).

The primary pure-surface-mode branches selected to be discussed here are S_1 and S_4, which persist into the long-wavelength regime and thus have elastic-continua analogs; S_6, which has peak amplitude in the first layer; the branches S_2, S_5, S_8, and S_3, all having peak amplitude in the second layer; and the branch S_7, which has peak amplitude in the *third* layer.

Inspection of Figs. 2 and 3 reveals that the usual effect of decreases in adatom mass is to raise surface-mode branches and that the usual effect of increases in M_L/M is to lower surface frequencies. The notable exceptions to this rule are branches having peak amplitude in the second or third layer: (a) S_5 and S_2 are hardly affected over the whole range of light to heavy adatoms reported here; (b) for increasing M_L, S_7 is not noticeably affected and S_8 and S_3 are only slightly more depressed (there *are* changes in the polarization character of S_3 in this case which are discussed below).

As is obvious from Figs. 2 and 3, there is a certain lack of symmetry between the effects of light adatoms and the effects of heavy adatoms. This asymmetry is, of course, a manifestation of dynamic decoupling (or lack thereof) in the sense of the adiabatic approximation.[22] Hence, for heavier adatoms the three principal adsorbed-layer surface wave branches S_1, A_2', and A_3'—associated in

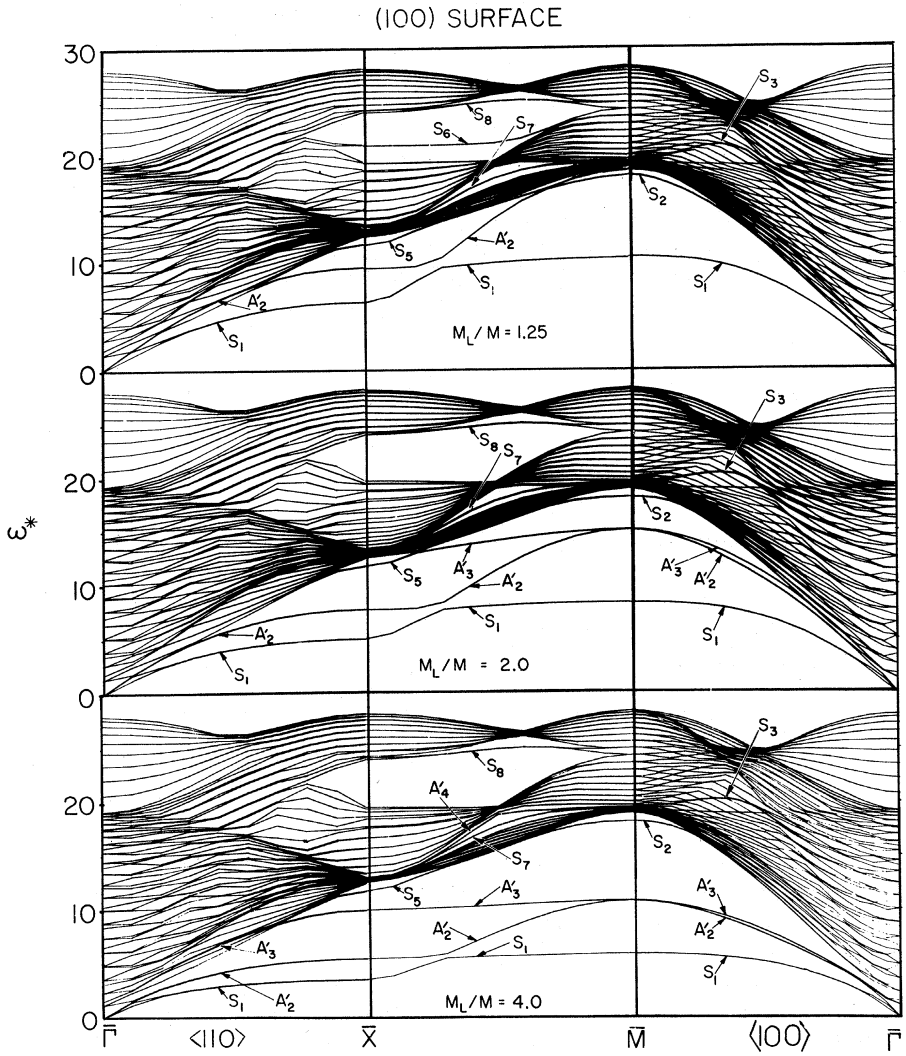

FIG. 3. Surface-dispersion curves of the fcc (100) slab, with adatom mass M_L greater than that of substrate atoms, M. The abscissa scale of the $\bar{M}\bar{\Gamma}$ segment is reduced by a factor of $2^{-1/2}$ relative to the other segments.

a sense with the three degrees of freedom of the adsorbed monolayer—exist over most of the DBZ. At the larger $\bar{q}$ values, the structure of this triplet of surface branches and the magnitude of the frequencies are somewhat similar to that of a single layer with atomic mass M_L. Here the adatoms, moving in their surface modes with long period due to their heavy mass, tend to drag along the first layer or so of the lighter substrate atoms, but with increasingly less response from the deeper substrate layers since the period is so much longer than that for the lowest natural period of the substrate. Thus the localization of S_1, A_2', and A_3' increases with increasing M_L (cf. discussion below of Fig. 4). When $\bar{q}$ is nearer the origin $\bar{\Gamma}$, the first two branches make a smooth transition to the behavior appropriate to the lowest surface and pseudosurface branches S_1 and S_4 appropriate to the pure surface. In this sense, the principal adsorbed-layer surface branches in the heavy adatom case can be considered as acoustical.

In the light adatom extreme, this dynamic decoupling yields principal adsorbed-layer surface branches which can be considered as optical; here the adatoms moving in their surface modes with short period due to their light mass tend to see the substrate of heavier atoms as an approximately static array of interaction centers, such that the principal adsorbed-layer surface branches A_1, A_2, and A_3 cannot tend to zero frequency as $\bar{q} \to 0$. For the lightest adatoms reported here, one branch A_3 exists over the whole DBZ; a second A_2 exists over most of the DBZ as a pure-surface branch and may be observed near $\bar{\Gamma}$ to continue into the bulk bands as a locus of mixed modes—which we shall call a pseudosurface branch[28]; and the third A_1 also exists in a region around $\bar{\Gamma}\bar{M}$ as a pure-surface branch which continues into the bulk band as a pseudosurface branch nearer $\bar{\Gamma}$. The $\bar{q} \to 0$ limit of all three surface and pseudosurface branches can be seen to be nonzero and hence optical.

The penetration of adsorbed-layer modes into the substrate bulk bands even for $M_L/M = 0.25$ means that the dynamic coupling between light layer and substrate is still quite appreciable at long wavelengths.[22] At much greater mass mismatches between adatoms and substrate atoms, one can expect the three surface branches associated with the monolayer to be completely separated from the bulk bands of the substrate (cf. results of Ref. 10 for $M_L/M = \frac{1}{56}$, simulating hydrogen on bcc iron). In such extreme cases, the adiabatic decoupling between the motions of the adsorbed layer and the substrate is more complete, and the three adsorbed-layer branches are approximately what would be expected of the atoms of the adsorbed layer moving in a potential field consisting of a contribution from the substrate atoms in a static configuration in addition to the mutual interaction of the adatoms. Thus, at $\bar{q} = 0$, the frequencies of the adsorbed-layer branches will be something like that of a single adatom interacting with a stationary substrate, with motion normal to the surface having a frequency somewhat greater than that for motion parallel to the surface (see the Appendix). As $\bar{q}$ increases, dispersion appears. The parts of the branches associated principally with vertical motion have relatively small dispersion. The parts of the branches associated principally with horizontal motion parallel to $\bar{q}$ exhibit quite large dispersion, rising to frequencies approximating those characteristic of longitudinal modes in bulk samples of the adatom species. Finally, the parts of the branches associated principally with horizontal motion transverse to $\bar{q}$ exhibit little dispersion when the direction of motion of an adatom is between its nearest neighbors in the substrate [for $\bar{q}$ along $\langle 110 \rangle$ for the fcc (100) surface and along $\langle 100 \rangle$ for the bcc (100) surface] and exhibit quite large dispersion when the adatom motion is toward its nearest neighbors in the substrate [$\bar{q}$ along $\langle 100 \rangle$ for the fcc (100) surface and along $\langle 110 \rangle$ for the bcc (100) surface].

Turning now to the discussion of the attenuation with depth of the surface modes, we begin with branch S_1 which persists in the long-wavelength limit. For materials with cubic-anisotropy ratio $\eta = 2c_{44}/(c_{11} - c_{12})$ less than unity, S_1 will exist well

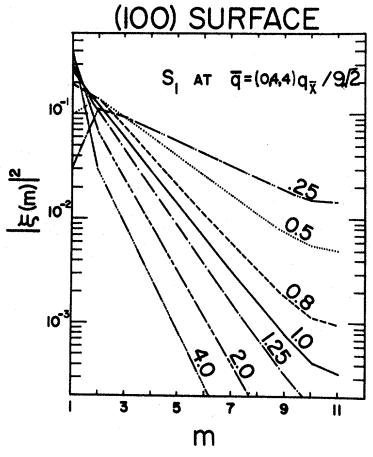

FIG. 4. Attenuation with depth of the mode S_1 of the fcc (100) slab for propagation in a $\langle 110 \rangle$ direction. The location of the mode plotted is marked by the S_1 arrow on the $\bar{\Gamma}\bar{X}$ segments of Figs. 2 and 3. $\vec{\xi}(m)$ is the mass-weighted amplitude [see Eqs. (2.6) and (2.9)], and m is the layer index, with $m = 1$ for the surface layer. The curves are labeled by values of the mass ratio M_L/M [$= M(1)/M(m), m > 1$]. (The plotted curve is the arithmetic average of the degenerate pair of modes on each branch. Note the logarithmic scale for $|\vec{\xi}|^2$.)

TABLE I. Attenuation constant α of the surface mode S_1 at $\bar{q}=[0,4,4]q_{\bar{X}}/9\sqrt{2}$ for different mass ratios in the adsorbed monolayer. α is defined by the relation $|\vec{\xi}(m)| = |\vec{\xi}(1)| \exp[-\alpha(m-1)]$.

M_L/M	α
4.0	0.295
2.0	0.255
1.25	0.208
1.0	0.183
0.8	0.1565
0.5	0.1075
0.25	0.0705

separated from the bulk band for all directions of propagation on a (100) surface and will have sagittal-plane polarization along both the ⟨100⟩ and ⟨110⟩ directions in the long-wavelength limit.[2] The case of materials having anisotropy ratio greater than unity, such as the present model ($\eta = 2.66$), differs in two respects: (i) Along ⟨100⟩ S_1 still has the sagittal-plane polarization, but along ⟨110⟩ S_1 is SH polarized (strictly normal to the sagittal plane); (ii) it appears that as the propagation direction approaches ⟨110⟩, S_1 becomes tangent to the bottom edge of the bulk band in the long-wavelength limit (i.e., in the long-wavelength regime, and as the propagation direction moves continuously toward ⟨110⟩, S_1 transforms smoothly into a pure-bulk shear wave propagating along the surface).[24] Figure 4 displays the attenuation with depth of S_1 for various mass ratios and at fixed wave vector $\frac{4}{9}$ of the way out to the point $\bar{X}$ of the DBZ (this point

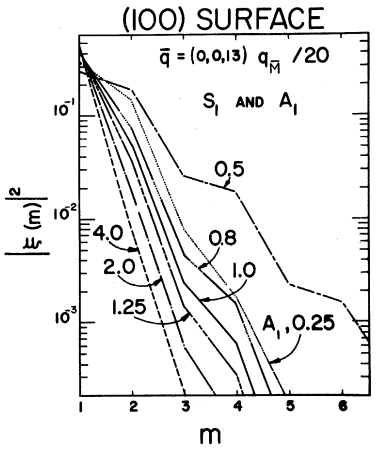

FIG. 5. Attenuation with depth of the mode S_1 and the mode A_1 of the fcc (100) slab for propagation in a ⟨100⟩ direction. Values of the mass ratio M_L/M label the curves. The location of the modes S_1 and A_1 plotted is marked by arrows in the $\bar{M}\bar{\Gamma}$ segments of Figs. 2 and 3.

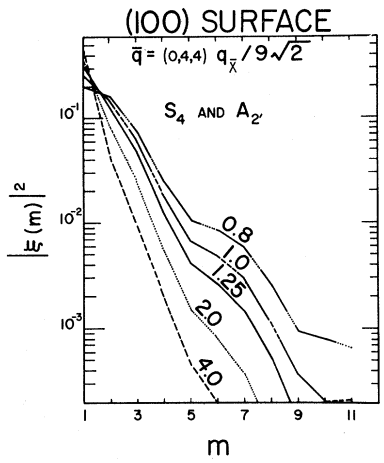

FIG. 6. Attenuation with depth of the mode S_4 and its heavy adatom alias A_2', for propagation in a ⟨110⟩ direction on the (100) face of a fcc slab. Values of the mass ratio M_L/M label the curves, and the locations of the modes are pointed out by arrows in the $\bar{\Gamma}\bar{X}$ segments of Figs. 2 and 3.

is located by the S_1 arrows in the left panel of Figs. 2 and 3). It is obvious that S_1 decays approximately exponentially at this wave vector for all mass ratios considered, and Table I gives the resulting attenuation parameter α vs the mass ratio. Heavier adatoms enhance localization of S_1, while lighter adatoms decrease localization of S_1, as was shown by Kaplan for a simple two-dimensional model.[5] In fact, for the lightest mass ratio, S_1 has been extinguished by being raised up into the bulk bands, and thus delocalized, along the entire DBZ boundary and over a sizable region extending into the interior of the DBZ. Figure 5 shows the localization of S_1 for wave vector along the cubic axis $\frac{13}{20}$ of the way to $\bar{M}$; here S_1 has been extinguished for $M_L/M = 0.25$, and in its place the localization of A_1 is shown. At this wave vector S_1 and A_1 no longer show an exponential decay from atomic layer to atomic layer; however, the attenuation curves do appear to have envelopes that decay exponentially. Again we see that the effect of the heavy adatom is to increase localization, and that the effect of the light adatom is toward delocalization. We should remark here that in the long-wavelength limit a monolayer has negligible effect on the surface waves of the pure surface, as found by Kaplan.[5]

Attenuation curves for the other surface branch persisting to long wavelengths—S_4 (and its alias A_2')—are presented in Fig. 6 for the same point in the DBZ as in Fig. 4. For the present model, having anisotropy ratio $\eta > 1$, S_4 lies embedded in the bulk band around the ⟨110⟩ direction in the long-wavelength region. Along ⟨110⟩, S_4 is polarized in the sagittal plane, while the bulk subband in which it is

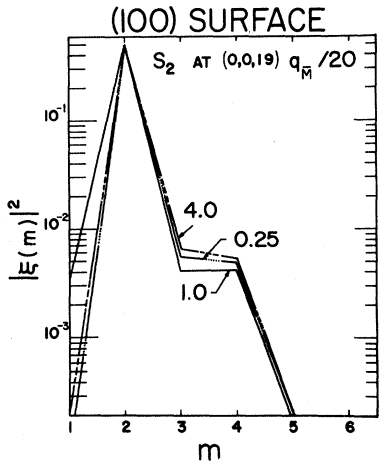

FIG. 7. Attenuation with depth of the mode S_2 for ⟨100⟩ propagation on the (100) face of a fcc slab. Values of M_L/M label the curves.

embedded is strictly SH polarized; hence S_4 is a pure-surface branch all along ⟨110⟩. (Away from ⟨110⟩, S_4 mixed with the background of bulk modes to yield a pseudosurface branch wherever it is not clear of the bulk band.) Although the attenuation curves of S_4 are more complex than those of S_1 at the same wave vector, the principal effect of varying the adatom mass is the same. A mass ratio somewhat less than 0.8 has extinguished S_4 at this point.

Before leaving the S_1 gap, we show in Fig. 7 attenuation curves for S_2 near the $\bar{M}$ point of the DBZ boundary. S_2 is the second-layer branch in the family of which S_1 is the first-layer branch.[25] The effect of the adsorbed layer on S_2 is quite minor, with the largest effect being reduction of amplitude for the adsorbed layer itself.

The behavior of the surface branches in the S_3 quasigap is intriguing. Musser and Rieder[19] have recently made an interesting study of the effects in the sagittal-plane modes along $\bar{\Gamma}\bar{M}$ arising from changes in the force constants at the surface. In the present work we see in Figs. 2, 3, and 8 that the second-layer branch S_3 does not shift much nor does its localization change much for our complete range of *heavy* adatoms. The case of light adatoms is in distinct contrast. For $M_L/M = 0.8$, S_3 has already been pushed out of the quasigap into the sagittal-plane subband and a new branch A_4 has been raised up into the quasigap. (It appears that A_4 may well be the mixed-mode branch M_1 in Fig. 10 of Ref. 2 raised up into the S_3 quasigap; at this mass ratio, A_4 has the same first-layer peak amplitude and principally P polarization as M_1 has for the pure surface.) At $M_L/M = 0.5$, A_4 has been further raised in the quasigap, such that it occupies a position approximating that of S_3 for the pure surface. The reason A_4 is more localized for $M_L/M = 0.5$ than for 0.8 is that at 0.8 it is just barely split from the bulk subband, whereas at 0.5 it is farther removed from edges of the subband.

Both S_3 and A_4 also undergo changes of character as they shift in the quasigap; these character shifts are related to the character of the bulk modes at the boundary of the quasigap. The quasigap is roughly triangular with both the horizontal bottom boundary and the inclined side nearest $\bar{\Gamma}$ associated with bulk waves of predominantly P polarization and with the inclined side nearest the DBZ boundary associated with bulk waves of predominantly SV polarization. The point for which Fig. 8 was plotted is in that region bounded above by SV bulk waves and below by P bulk waves. S_3, although not greatly shifted downward by increasing M_L/M, does shift far enough that its polarization ellipse transforms from the predominantly SV character obtained for the pure surface to the predominantly P polarization characteristic of the bottom edge of the quasigap. For decreasing values of M_L/M, A_4 changes from P for 0.8 to SV for 0.5.

As a final example of the effect of an adsorbed layer on a surface mode of the (100) surface, we show attenuation curves for S_8 at a point on the boundary of the DBZ. (see Fig. 9). Heavier masses only slightly shift S_8 farther into the S_6 gap and increase localization. Lighter masses have a greater effect—S_8 is quickly pushed up into the bulk band and extinguished.

The details of connectivity of the surface branches in Figs. 2 and 3 are quite complicated. Nevertheless, gross features of the shift with adatom mass of many of the surface branches can be encompassed by the following viewpoint: As the adatom mass

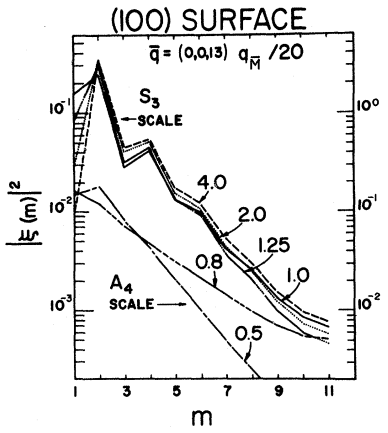

FIG. 8. Attenuation with depth of the mode S_3 (four mass ratios) and the mode A_4 (two mass ratios) for ⟨100⟩ propagation on the (100) face of a fcc slab. Values of M_L/M label the curves. For clarity of presentation, the vertical scale has been shifted for A_4. Arrows locate these modes on the $\bar{\Gamma}\bar{M}$ segments of Figs. 2 and 3.

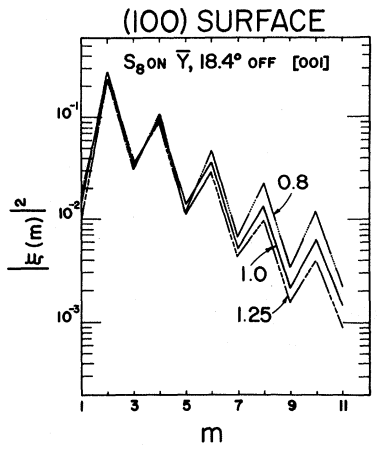

FIG. 9. Attenuation with depth of the mode S_8 for propagation in a direction 18.4° off a ⟨100⟩ axis in the (100) face of a fcc slab. The mode is located by an arrow in the $\bar{X}\bar{M}$ segments of Figs. 2 and 3. Values of M_L/M label the curves.

is decreased from the heavy adatom extreme, the principal adsorbed-layer surface branches are raised up, moving into the bulk bands (and being completely, or sometimes only partially, delocalized), making transits through the various gaps as they are encountered, and finally, in the light adatom extreme, appearing completely above the bulk bands. One can follow these transits through the bulk bands by the principal adsorbed-layer surface branches for the other two surfaces discussed below.

B. (111) Surface

Figures 10 and 11 display surface-dispersion curves for the fcc (111) surface for light adatoms (Fig. 10) and heavy adatoms (Fig. 11). The bulk bands of the (111) surface are less complex than those for (100) or (110). There do not seem to be any quasigaps such as the S_3(100) quasigap. There are four gaps—the trivial S_1 gap, the large S_2 gap, the smaller S_3 gap, and the tiny S_4 gap (A_4' in Fig. 11)—and except for the last these are quite simply related to the three branches of dispersion curves for propagation directions in a (111) plane in the bulk. The principal symmetry directions in a (111) plane are ⟨110⟩ and ⟨211⟩, and only along the ⟨211⟩ directions is the sagittal plane one of mirror symmetry such that the modes partition into two-thirds of the modes being elliptically polarized in the sagittal plane and one-third of the modes strictly SH polarized. For the pure surface, the only second-layer mode observed is in a very small region near $\bar{K}$—so small that it cannot be resolved in the figure; the paucity of second- and higher-layer modes is partly due to the small relaxation at a free (111) surface.[2,14] Finally, the pure surface possesses a fairly well-defined pseudosurface branch MS_3 which is not labeled in the adsorbed-layer figures, but which appears as a well-defined feature in the midregion of $\bar{K}\bar{\Gamma}$ for $M_L/M = 1.25$. For the pure surface, MS_3 appears in some sense to be a continuation of S_3 into the bulk band along $\bar{K}\bar{\Gamma}$, but the continuation is very indistinct in the dense part of the bulk subband at the lower edge of the S_3 gap. Thus, in a scattering picture MS_3 would be a fairly sharp resonance near the middle of $\bar{K}\bar{\Gamma}$, but it would broaden to the point of becoming lost near the edge of the S_3 gap.

The surface branches existing for the pure surface are quite close to the tops of the gaps in which they are located. Consequently, they are readily extinguished by a monolayer of light adatoms. For $M_L/M = 0.8$, only S_1 still exists, and a new adsorbed-layer branch A_3 is beginning to make an appearance at the extreme top of the bulk bands. At mass ratio 0.5 even S_1 has been extinguished over much of the DBZ. Here A_3 is a pure surface branch over most of the DBZ and a pseudosurface branch continuation of A_3 can be discerned readily. A new surface branch A_2 has appeared; it is mixed where it would cross the bulk subband above the S_2 gap, but it exists as a strict surface branch well into the bulk subbands along $\bar{\Gamma}\bar{M}$, since its SH polarization is decoupled from the sagittal-plane polarized bulk subband it first enters. At $M_L/M = 0.25$, the principal adsorbed-layer surface branches A_3, A_2, and A_1 exist above the bulk bands over most of the DBZ. The adsorbed-layer modes for predominantly vertical motion exist over the entire DBZ, as the largely horizontal portions of A_1, A_3, and A_2. Quite noticeable hybridization appears where the adsorbed-layer branches for predominantly horizontal motion would cross the relatively dispersionless branch for vertical motion; hence, only along $\bar{\Gamma}\bar{M}$ does branch A_2 actually cross A_1. The pseudosurface-branch continuations of A_2 and A_3 into the bulk bands are quite apparent, especially along $\bar{K}\bar{\Gamma}$. Finally, new surface branches have appeared in the S_2, S_3, and S_4 gaps, while S_1 exists only near $\bar{\Gamma}$.

For increasing mass ratios, surface branches are depressed, with the surface branches existing in the intraband gaps for the pure surface making complete transits through these gaps, and new surface branches peeling down from the tops of the gaps to follow them. Since the S_4 gap is so narrow, the S_4 branch is the first to complete a transit through its gap; by the time $M_L/M = 1.25$ has been reached, S_4 has been pushed all the way through the S_4 gap and is no longer observable, and another branch A_4' has been split off the top of the S_4 gap. A_4' persists to a mass ratio of 2.0, but at a mass ratio of 4.0 even it has been pushed down into the bulk band and lost.

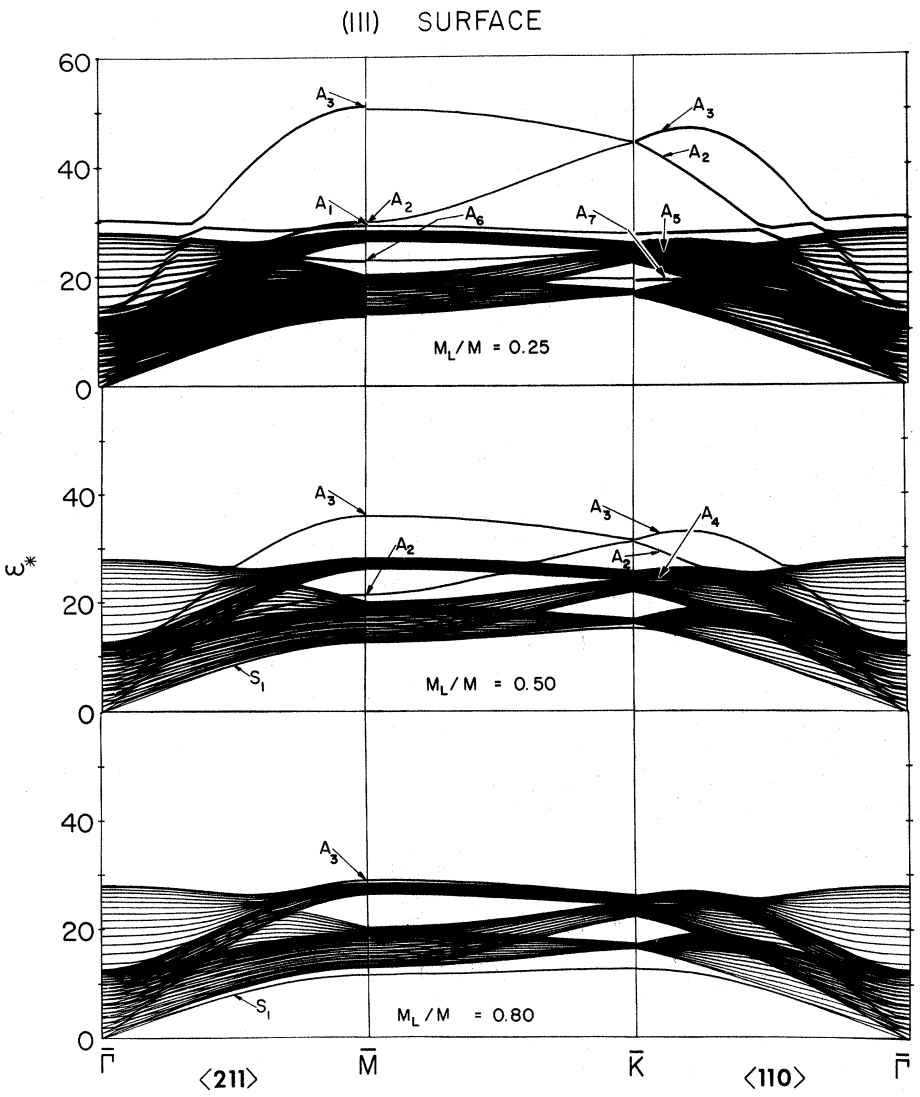

FIG. 10. Surface-dispersion curves of the fcc (111) slab, with $M_L/M < 1$. Relative to the $\bar{\Gamma}\bar{M}$ segment, the abscissa scale of the $\bar{M}\bar{K}$ segment has been expanded by a factor of $\sqrt{3}$ and that of the $\bar{K}\bar{\Gamma}$ segment has been reduced by a factor of $\frac{1}{2}\sqrt{3}$.

Several other interesting features have also developed at a mass ratio of 1.25. S_3 has been pushed down to about the middle of its gap, and a new branch A_5' has been split off the top of the S_3 gap to a position below that of S_3 for the pure surface. A_5' can be seen to be continued into the bulk subband between $\bar{M}$ and $\bar{K}$ as a pseudosurface branch. It appears that A_5' may be associated with S_2. Furthermore, one can observe a feature in the bulk band which appears to be a pseudosurface branch which may be associated with A_5' in about the same way as S_2 is. The branch S_3 can be seen penetrating into the bulk bands as a pseudosurface branch along $\bar{K}\bar{\Gamma}$ for a short distance. However, the association between S_3 and the pseudosurface branch MS_3, which seems so direct in the case of the pure surface,[2] is here somewhat more complicated. At the mass ratio of 1.25, a new surface branch A_2' has made an appearance near $\bar{M}$ and $\bar{K}$, and it is not clear whether MS_3 (seen here as a distinct feature in the lowest sparsely populated bulk band from $\bar{\Gamma}$ to near the middle of $\bar{K}\bar{\Gamma}$) should be considered as a continuation of S_3 or A_2'.

At the mass ratio of 2.0, the question of the association of MS_3 no longer exists. A_2' now exists over most of the DBZ, and it is quite clearly seen to penetrate into the bulk band along $\bar{K}\bar{\Gamma}$ as the pseudosurface branch that was MS_3 in the case of the pure surface. Also at this mass ratio a new surface branch A_3' has appeared near $\bar{K}$, where it can be seen to penetrate into the bulk band as a pseudosurface branch visible as a feature lying somewhat above the position of MS_3 for the pure surface. It may, in fact, be useful to consider A_2' as S_3 pushed all the way through the bulk subband below the S_3 gap. (Although reduction of Fig. 11 for publication may wash out this detail, on the original for Fig. 11 a pseudosurface-branch con-

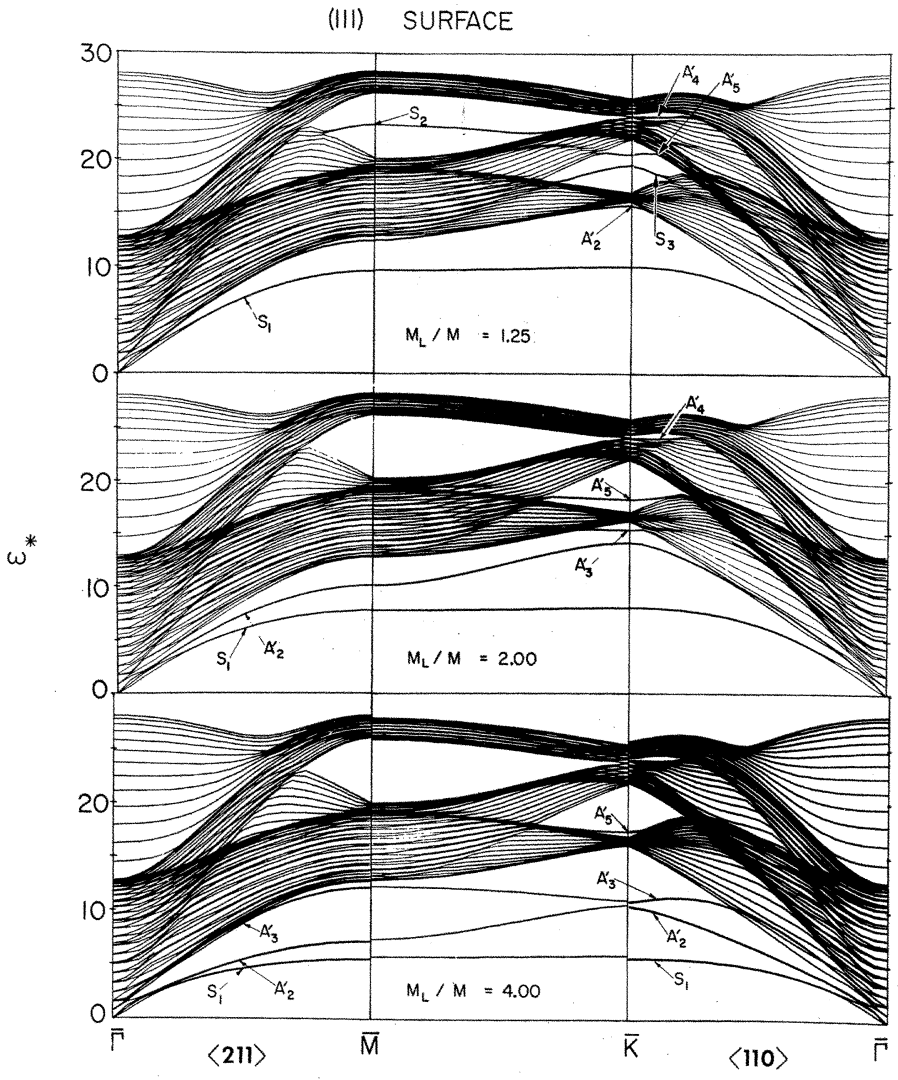

FIG. 11. Surface-dispersion curves of the fcc (111) slab, with $M_L/M > 1$. Relative to the $\bar{\Gamma}\bar{M}$ segment, the abscissa scales of $\bar{M}\bar{K}$ and $\bar{K}\bar{\Gamma}$ have been multiplied by factors of $\sqrt{3}$ and $\frac{1}{2}\sqrt{3}$, respectively. (The slight discontinuities at $\bar{M}$ and $\bar{K}$ in the bottom panel resulted from small variations in plotter calibration and have no physical significance.)

tinuation of A_3' can be seen in the densely populated transverse bulk subbands along $\bar{\Gamma}\bar{M}$.) A further increase in mass to $M_L/M = 4.0$ brings A_3' clear of the bottom edge of the bulk bands over much of the DBZ to complete the set S_1, A_2', and A_3', the three principal adsorbed-layer surface branches. Along $\bar{K}\bar{\Gamma}$, the pseudosurface-branch continuation of A_3' into the lower bulk subband is obvious.

An over-all qualitative picture of localization of vibrations near the surface can be obtained from an effective frequency distribution $f_\alpha(\omega; m)$ for each atomic layer and each direction of vibration, defined such that[2,26]

$$f_\alpha(\omega; m)\,d\omega = (1/\bar{N}) \sum_{\omega \le \omega' < \omega + d\omega} |\xi_\alpha(m; \omega')|^2 , \qquad (3.1)$$

That is, the contribution of a frequency to $f_\alpha(\omega; m)$ is weighted according to how much the corresponding vibrational mode is represented in the mth layer and the α direction. [The number of particles per atomic plane in the slab $\bar{N}$ is inserted to normalize $f_\alpha(\omega; m)$.] In Fig. 12, we exhibit effective frequency distributions for 21 atomic-layer slabs for $M_L/M = 0.20$, 0.5, 0.8, 1.0, and 2.0. The solid line is $f_\perp(\omega; m) \equiv f_z(\omega; m)$, i.e., the effective distribution for motions normal to the surface. The dotted line is $f_\parallel(\omega; m)$, the effective distribution for motions parallel to the surface:

$$f_\parallel(\omega; m) \equiv f_x(\omega; m) = f_y(\omega; m) . \qquad (3.2)$$

The pure-surface case, $M_L/M = 1.0$, is discussed in Ref. 2, and we include it here as a standard of reference for the effects of the adsorbed layer. We note first that the $f_\alpha(\omega; 11)$, the effective distributions for the central layer, differ very little in all cases; in fact, they very closely approximate the total distribution for the bulk of the substrate material.

The association of the detailed structure of the $f_\alpha(\omega; m)$ with the various surface branches is somewhat complicated by the fact that over so much of the DBZ the polarizations are quite elliptical. However, it is quite easy to see that for $M_L/M = 2.0$ the Rayleigh wave peak in the vertical direction in the first layer has been pushed to lower frequencies. At this mass ratio, too, the vertical motion in the second layer associated with A_5' can be seen in the largest peak in the interval just below $\omega^* = 20$. As the mass ratio is decreased from unity, in $f_\perp(\omega; 1)$ one can see first the upward shift of the Rayleigh branch S_1, then the extinction of S_1 over most of the DBZ, and finally the flat portions of the adsorbed-layer surface branches that exist over the whole DBZ.

C. (110) Surface

Inspection of the surface-dispersion curves for an adsorbed layer on the fcc (110) surface (shown in Figs. 13 and 14) shows that this is the most complex case. In this paper, we shall limit the discussion to only the more general points.

The principal features of the bulk bands for the (110) surface are the S_1, S_7, and S_5 gaps. The latter two are homologous to each other and to the S_2 (100) gap in that their general configurations are similar—including bottlenecks in the bulk subband above them.[2]

As was the case for the (100) surface, the second-layer surface branches associated with the top of the gaps—S_8, S_6, and S_4 for the (110) surface—are relatively little shifted over the range of mass ratios for the heavy adatoms considered here. On the other hand, the branch S_5, although having second-layer character along and near the DBZ boundary $\overline{SY}$, responds to increasing adatom mass by large downward shifts in the same way as the first-layer surface branches S_7 (to which S_5 is somewhat homologous), S_3, S_2, and S_1. This behavior reinforces the notion that the S_5 second-layer character along $\overline{SY}$ is not of the same origin as that of S_8 and S_6, and is very likely due to a complex interaction with the modes in the bulk band containing the pseudosurface branch MS_7 along $\overline{SY}$.[2] This pseudosurface branch MS_7 may still be seen for $M_L/M = 1.25$ as a feature extending down and to the right from the S_7 label at $\overline{S}$ (at $\overline{S}$, the MS_7 motions decouple through symmetry from the background of bulk modes). For $M_L/M = 2.0$, MS_7 has been pushed down into the denser part of the bulk band and is delocalized, except at $\overline{S}$ where it is still observable as a mixed mode.

For $M_L/M = 4.0$, the three principal acoustical-surface branches S_1, S_2, and S_3 exist clear of the bulk band over almost all of the DBZ. [For the (110) surface, the S labels have been retained for branches 2 and 3 instead of using A_2' and A_3', because all three principal branches are observable for the pure surface.[2]] Along $\overline{Y\Gamma}$, S_1 is principally

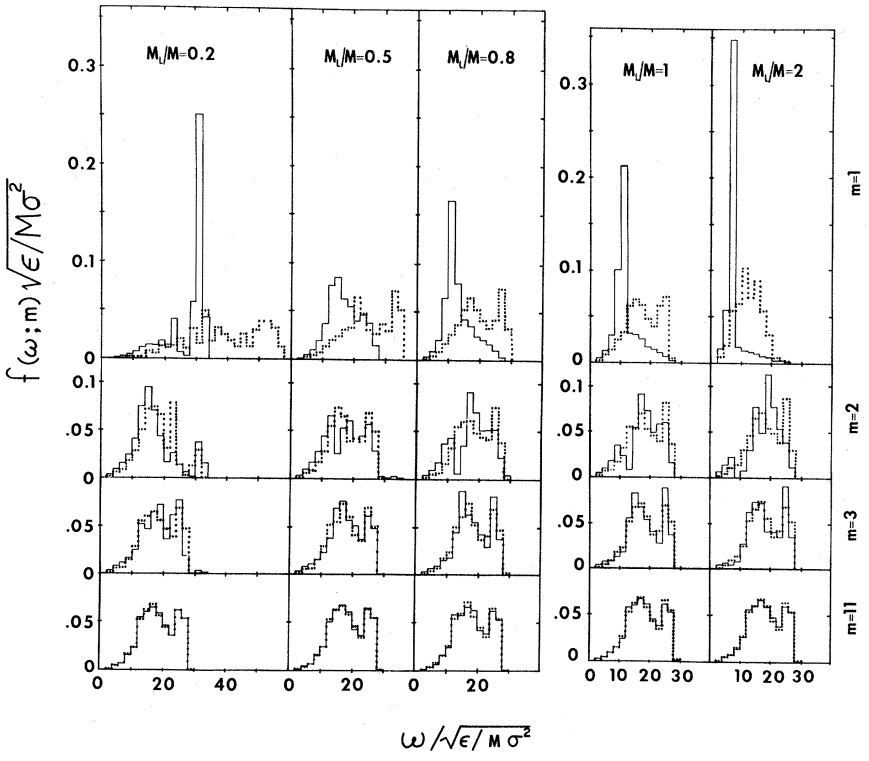

FIG. 12. Effective distribution of frequencies by polarization component and atomic plane, $f_\alpha(\omega; m)$, for a fcc (111) slab. The solid histogram is $f_\perp(\omega; m)$, and the dotted histogram is $f_\parallel(\omega; m)$. Each histogram is normalized to unit area. Distributions for the outer three planes ($m = 1, 2, 3$) and the center plane ($m = 11$) of a 21-plane slab are shown.

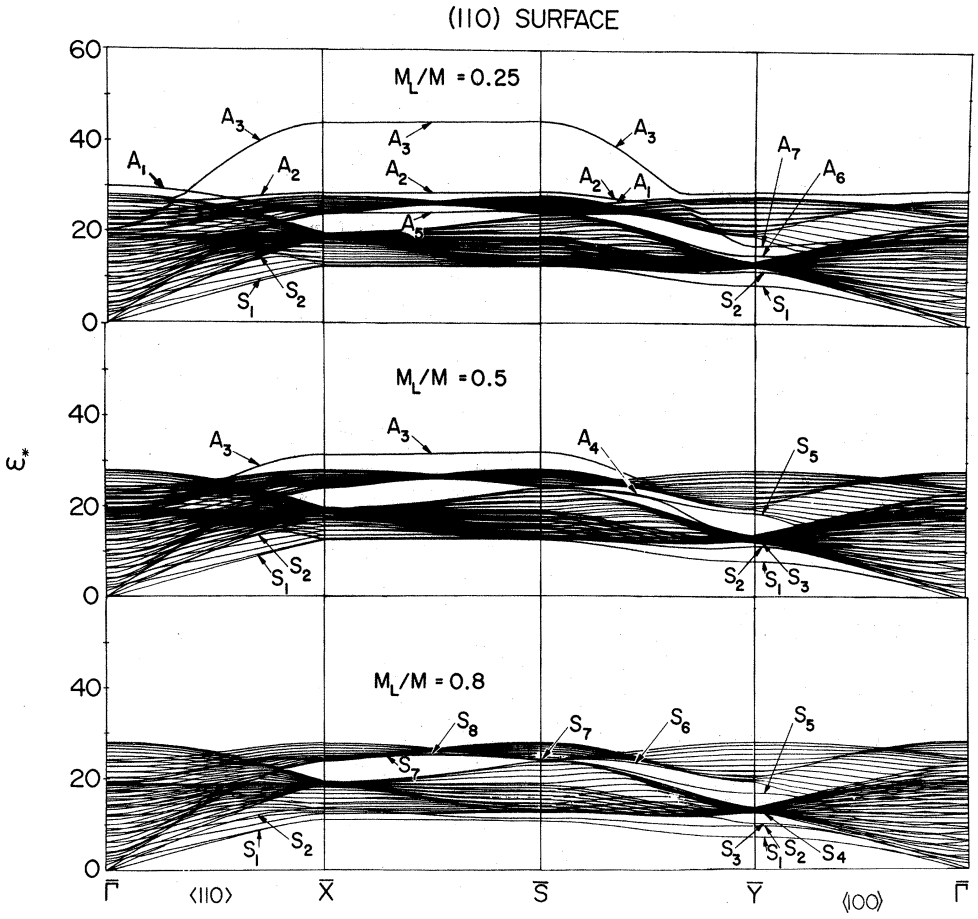

FIG. 13. Surface-dispersion curves of the fcc (110) slab, with $M_L/M < 1$. Relative to the $\bar{\Gamma}\bar{X}$ and $\bar{S}\bar{Y}$ segments, the abscissa scale of the $\bar{X}\bar{S}$ and $\bar{Y}\bar{\Gamma}$ segments has been expanded by a factor of $\sqrt{2}$.

longitudinal in the first layer, S_2 is strictly SH, and S_3 is principally vertical in the first layer. Along $\bar{S}\bar{Y}$, one can see the hybridization between S_2 and S_3 just to the left of $\bar{Y}$. Farther along $\bar{X}\bar{S}\bar{Y}$, hybridization between S_1 and S_2 takes place, so that along $\bar{\Gamma}\bar{X}$ the principally vertical polarization in the first layer winds up on S_1, S_2 has recovered strict SH polarization, and S_3 is now principally longitudinal in polarization.

As the adatom mass is decreased (Fig. 13), we see that the second-layer surface branches S_8, S_6, and S_4 are quickly extinguished. The in-gap surface branch S_5 can be seen to respond much more slowly than the somewhat related branch S_7; S_7 is quickly raised into the bulk bands and does not appear for $M_L/M = 0.5$. For $M_L/M = 0.5$, S_5 coexists in its gap with a new surface branch A_4, and no surface branch appears in the S_7 gap.

For the lightest adatom mass studied for this surface, a new surface branch A_5 has been raised into the S_7 gap; it appears as if it is a continuation of the adsorbed-layer branch A_1 above the bulk bands. S_5 has been extinguished, and in its gap are two branches A_7, purely SH polarized along $\bar{Y}\bar{\Gamma}$, and A_6, having peak amplitude in the third layer and principally vertical polarization in this layer (at the $\bar{q}$ point where the A_7 and A_6 labels appear in Fig. 13). It appears likely that A_7 is A_4 shifted upward. A_7 can be seen to penetrate as a pure-surface branch into the sagittally polarized bulk subband toward $\bar{\Gamma}$ and to penetrate as a pseudo-surface branch up through the bulk band along $\bar{S}\bar{Y}$ to become the optical branch A_1. Considerable evidence of hybridization between A_1 and A_3 appears where A_1 emerges from the bulk band along $\bar{S}\bar{Y}$.

For $M_L/M = 0.25$, the principal optical-adsorbed-layer branches for the (110) surface are entangled in the bulk bands to a greater extent than they are for the (100) and (111) surfaces. This feature is due to the relative openness of this surface. Even so, one can see evidence of the hybridization between the three principal surface branches in much the same way as seen for the pure surface and the heavy adatom case. Along $\bar{Y}\bar{\Gamma}$, the first-layer polarization of the flat portion of A_3 is principally longitudinal; along $\bar{\Gamma}\bar{X}$, this flat portion is strictly SH and is labeled A_1 because it crosses A_3 along this symmetry direction. Along $\bar{\Gamma}\bar{X}$, A_3 is principally longitudinal and is seen first as a pseudo-surface branch near $\bar{\Gamma}$ and then as a surface branch

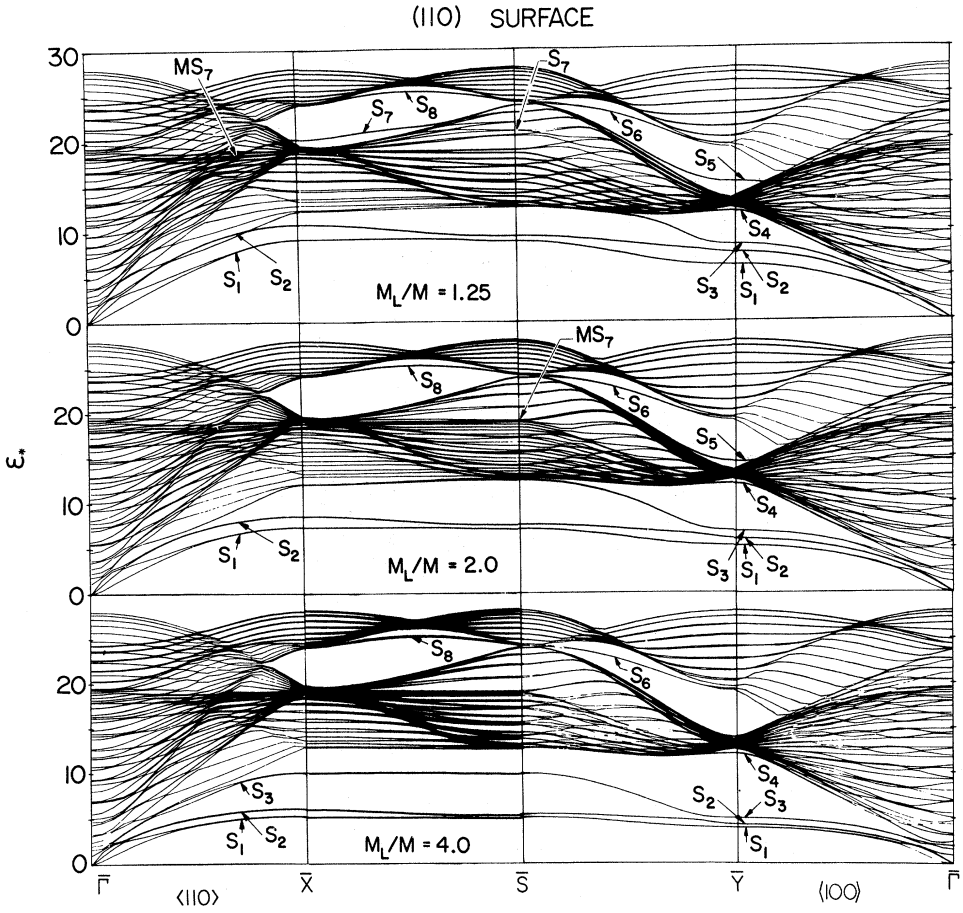

FIG. 14. Surface-dispersion curves of the fcc (110) slab, with $M_L/M > 1$. Relative to the segments $\bar{\Gamma}\bar{X}$ and $\bar{S}\bar{Y}$, the abscissa scale of $\bar{X}\bar{S}$ and $\bar{Y}\bar{\Gamma}$ has been expanded by a factor of $\sqrt{2}$.

rising to the highest frequency at $\bar{X}$. Also along $\bar{\Gamma}\bar{X}$, we see the flat principally vertically polarized branch A_2 appears and crosses A_1. The pseudosurface-branch continuation of A_2 back toward $\bar{\Gamma}$ is not as readily apparent but does exist as a feature back to $\omega^* \approx 27$ at $\bar{\Gamma}$; its hybridization with A_3 occurs in the neighborhood of the emergence of A_3 from the bulk band.

IV. CONCLUSION

The purpose of this paper was to explore the surface-localized and quasilocalized modes of fcc crystal surfaces bearing a monolayer of adsorbed atoms. In particular, the study of the effect of the adsorbed monolayer on the surface modes of the pure surfaces was an important objective, since it was found in Ref. 2 that the surface-mode spectra of such surfaces are remarkably complex. The study was carried out by simulating the adsorbed monolayer with a simple mass-defect model.

We find that there are three principal surface branches associated with the adsorbed monolayer in both extremes of light or heavy adatoms. Over most of the DBZ, these principal branches have configurations reminiscent of the configuration of the respective bulk bands but with frequencies roughly proportional to $(M_L/M)^{-1/2}$. In the long-wavelength limit, however, the heavy adatom principal surface branches are acoustical in that they smoothly go over into the branches for the pure surface having a zero-frequency limit as $\bar{q} \to 0$. The light adatom principal surface branches are optical in that their long-wavelength limits have nonzero frequency. Many of the surface branches seen in the bulk band gaps and the pseudosurface branches seen within the bulk bands in the intermediate stages of transition from the heavy to the light adatom extreme can be considered as parts of the three principal adsorbed-layer surface branches in transit through the bulk bands.

The surface branches having peak amplitude beneath the outer layer are observed to be relatively insensitive to the presence of heavy adatoms; in the opposite case of light adatoms, these subsurface surface branches are quickly extinguished, with a few notable exceptions. On the other hand, the surface branches having peak amplitude in the first layer are always shifted significantly by the presence of a monolayer (except in the long-wavelength limit for the acoustical branches). In partic-

ular, the generalized Rayleigh wave S_1 is extinguished for sufficiently light adatoms except in a small region near $\bar{q}=0$.

APPENDIX

Here we justify the assertion in Sec. III that for $\bar{q}=0$ the frequency associated with the vertical motion of a light adatom is significantly greater than that associated with horizontal motion. To do so, we consider the following model: a single adatom in the field of four stationary substrate atoms. The substrate atoms lie on the corners of a square of diagonal length $2b$, and the equilibrium position of the adatom is taken to be a distance $b+\delta$ (where $|\delta/b| \ll 1$) above the center of the square. The adatom interacts with the substrate atoms through a pairwise central potential $\phi(r)$ so that the total potential of the adatom is

$$\Phi(x,y,z)=\sum_{i=1}^{4}\phi(r_i)\,, \tag{A1}$$

where

$$r_{1,3}=[(x\pm b)^2+y^2+(z+b+\delta)^2]^{1/2}\,,$$
$$r_{2,4}=[x^2+(y\pm b)^2+(z+b+\delta)^2]^{1/2}\,, \tag{A2}$$

with (x, y, z) being the displacement from equilibrium.

The equilibrium condition may easily be shown to be

$$\phi'(r_0)=0\,, \tag{A3}$$

where

$$r_0=[b^2+(b+\delta)^2]^{1/2} \tag{A4}$$

is the equilibrium distance between the adatom and one of the substrate atoms.

The force constants governing the harmonic motion of the adatom for small displacements from equilibrium are then

$$\Phi^0_{xx}=\Phi^0_{yy}=2(b/r_0)^2\phi''(r_0)\,, \tag{A5}$$

$$\Phi^0_{xy}=\Phi^0_{xz}=\Phi^0_{yz}=0\,, \tag{A6}$$

$$\Phi^0_{zz}=4[(b+\delta)/r_0]^2\phi''(r_0)\,. \tag{A7}$$

Comparing Eqs. (A5) and (A7), we see that the frequency of the z vibration will be significantly greater than that of the x vibration. That the calculations reported in Sec. III and in Ref. 10 do not give the frequency ratio of $\sqrt{2}$ found in this simple model is a reflection of the facts that there *is* coupling between substrate and adatom motions and that there are interactions from second- and higher-order neighbors.

If one considers an adatom occupying a vacancy position *in* the first layer of the substrate, one finds that the order of the frequencies of vertical and horizontal motions is reversed[10] because the four additional neighbors in the same plane as the adatom greatly stiffen the horizontal restoring force while making no addition to the vertical restoring force. Extending the above model to describe this case, one finds for the force constants

$$\Phi^0_{xx}=\Phi^0_{yy}=2(b/r_0)^2\phi''(r_0)+4(b/\rho_0)^2$$
$$\times[\phi''(\rho_0)-\rho_0^{-1}\phi'(\rho_0)]+4\rho_0^{-1}\phi'(\rho_0)\,, \tag{A8}$$

$$\Phi^0_{xy}=\Phi^0_{xz}=\Phi^0_{yz}=0\,,$$

$$\Phi^0_{zz}=4[(b+\delta)/r_0]^2\phi''(r_0)\,,$$

where $\rho_0=(2b^2)^{1/2}$ is the equilibrium distance between the adatom and one of its nearest-neighbor substrate atoms in the same plane and where the other quantities are as defined previously. Since ρ_0 is only slightly smaller than r_0, $\phi'(\rho_0)$ is negative and very close to zero. Thus,

$$\Phi^0_{xx}\approx\Phi^0_{zz}+2(b/r_0)^2\phi''(r_0)\,,$$

and the x motions will have a higher frequency than will the z motions.

---

*Research sponsored by the Air Force Office of Scientific Research, Office of Aerospace Research, USAF, under Grant Nos. AFOSR-71-1973 and AFOSR-1257-67.

†Present address: Department of Physics, Texas A & M University, College Station, Texas 77843.

[1]R. E. Allen, G. P. Alldredge, and F. W. de Wette, this issue, Paper I, Phys. Rev. B 4, 1648 (1971).

[2]R. E. Allen, G. P. Alldredge, and F. W. de Wette, preceding paper, Paper II, Phys. Rev. B 4, 1661 (1971).

[3]J. Hori and T. Asahi, Progr. Theoret. Phys. (Kyoto) 31, 49 (1964).

[4]T. Asahi and J. Hori, in *Proceedings of the International Conference on Lattice Dynamics, Copenhagen,* 1963, edited by R. F. Wallis (Pergamon, Oxford, 1965), p. 571.

[5]H. Kaplan, Phys. Rev. 125, 1271 (1962).

[6]A. Corciovei and D. Vamanu, J. Vacuum Sci. Tech. 6, 680 (1969); references to the earlier work by Corciovei and co-workers are given in this paper.

[7]J. Dlouha, Czech. J. Phys. B16, 495 (1966).

[8]O. Litzman and V. Janku, Surface Sci. 18, 357 (1969); O. Litzman, Czech. J. Phys. B18, 1587 (1968).

[9]L. Dobrzynski and D. L. Mills, J. Phys. Chem. Solids 30, 1043, 2797 (1969).

[10]L. Dobrzynski, Surface Sci. 20, 99 (1970).

[11]W. Ludwig and B. Lengeler, Solid State Commun. 2, 83 (1964); D. C. Gazis and R. F. Wallis, Phys.

Rev. 151, 578 (1966); 156, 1038 (1967).

[12]R. E. Allen, G. P. Alldredge, and F. W. de Wette, J. Chem. Phys. 54, 2605 (1971).

[13]R. E. Allen, G. P. Alldredge, and F. W. de Wette, Phys. Rev. Letters 23, 1285 (1969); 24, 301 (1970); G. P. Alldredge, R. E. Allen, and F. W. de Wette, Bull. Am. Phys. Soc. 15, 101 (1970).

[14]R. E. Allen and F. W. de Wette, Phys. Rev. 179, 873 (1969).

[15]Two-dimensional vectors having only x and y components are denoted by roman type with superior bars; see Ref. 1.

[16]The lowest edge of the bulk bands is not necessarily given by the lowest bulk wave with $\vec{q}=\bar{q}$. See, e.g., Ref. 18.

[17]Intrabulk band gaps have not been reported in the papers dealing with the simple-cubic structure. However, gaps are probably the rule in fcc and bcc, since they appear not only in the work on fcc using the present model (Refs. 13 and 2) but also in work on bcc iron (Ref. 10).

[18]G. P. Alldredge, R. E. Allen, and F. W. de Wette, J. Acoust. Soc. Am. 49, 1453 (1971).

[19]S. W. Musser and K. H. Rieder, Phys. Rev. B 2, 3034 (1970); S. W. Musser, J. Phys. Chem. Solids 32, 115 (1971).

[20]Interestingly, $S_7(100)$, which is a *third*-layer surface mode, persists when the surface force constants are given their bulk value, whereas $S_3(100)$, which is a *second*-layer surface mode, disappears for bulk values of the surface force constants.

[21]See, e.g., P. M. Morse, in *Handbook of Physics*, edited by E. U. Condon and H. Odishaw (McGraw-Hill, New York, 1967), Pt. 3, Chap. 7.

[22]These remarks on "dynamic decoupling in the adiabatic sense" are meant to be taken only as a heuristic roughly approximate analogy to the adiabatic (Born-Oppenheimer) approximation separating electronic and nuclear motions in the quantum mechanics of molecular systems [cf. M. Born and K. Huang, *Dynamical Theory of Crystal Lattices* (Oxford U. P., Oxford, 1954), Sec. 14]. The quality of the approximation is fairly good for the frequencies, but as in the analogous case in quantum mechanics the true eigenvectors are less well represented by the approximate picture.

[23]Strictly speaking, in the present method of studying surface vibrations by calculating the normal modes of a finite crystalline slab, surface branches hybridize considerably with the bulk branches of most bulk bands through which they pass. The result is disappearance of the surface branch as such, leaving behind a locus of mixed modes through the bulk band. Since in a scattering picture of a semi-infinite crystal such loci of mixed modes would be branches of modes only resonantly localized at the surface, we refer to such loci as pseudosurface branches.

[24]See G. W. Farnell, in *Physical Acoustics*, Vol. 6, edited by W. P. Mason and R. N. Thurston (Academic, New York, 1970).

[25]S_2 and S_5 are separately labeled because they have different character (SV and SH, respectively); S_1 and S_4 interchange character between ⟨110⟩ and ⟨100⟩ where it appears they are the result of hybridization between a SH surface branch and a SV surface branch (cf. Refs. 2 and 18).

[26]R. E. Allen, G. P. Alldredge, and F. W. de Wette, Phys. Rev. B 2, 2570 (1970).

PHYSICAL REVIEW B VOLUME 4, NUMBER 6 15 SEPTEMBER 1971

Quantum Mobility and Nuclear-Spin-Echo Damping in Impure Crystals

Allan Widom
Physics Department, Northeastern University, Boston, Massachusetts 02115
(Received 11 May 1971)

Dash has attributed the low-temperature loss of configurational entropy in impure crystals to the quantum mobility of the impurities. The resulting specific-heat peaks at $T=\Delta/k_B$ have not yet been observed, probably owing to the extremely small values of the mobility bandwidths Δ. In this paper it is shown that if $\Delta \gg \hbar(D^2g/a^3)^{1/3}$, then the mobility bandwidth can be measured via nuclear-spin-echo-damping experiments carried out at temperatures much larger than Δ/k_B. D is the diffusion coefficient, a is the lattice spacing, and $\vec{g}$ is the magnetic-field gradient (measured in frequency units). The damping factor is shown to have an oscillatory character in this limit as opposed to the usual classical $e^{-Dg^2t^3/12}$ form. Practical limits to the method yield $\Delta/k_B \gtrsim 10^{-5}$ °K as an approximate lower bound on detectable widths.

I. INTRODUCTION

Consider the ground-state wave function of a single impurity atom in an otherwise perfect crystal. Let N_s be the number of equivalent binding sites for the impurity. If the impurity were immobile, then the ground state would be N_s-fold degenerate. Furthermore the ground-state degeneracy of a dilute solid solution of $N \ll N_s$ impurities would be[1]

$$\Gamma \simeq N_s^N/N! \,. \tag{1}$$

This gives rise to a macroscopic ground-state configurational entropy

$$S_c = k_B \ln\Gamma \,, \tag{2}$$